Japanese Journal of Applied Physics **55**, 05FF06 (2016)
http://doi.org/10.7567/JJAP.55.05FF06

REGULAR PAPER

Sub-230 nm deep-UV emission from GaN quantum disks in AlN grown by a modified Stranski–Krastanov mode

SM Islam[1], Vladimir Protasenko[1], Sergei Rouvimov[2], Huili (Grace) Xing[1,3], and Debdeep Jena[1,3*]

[1]*School of Electrical and Computer Engineering, Cornell University, Ithaca, NY 14853, U.S.A.*
[2]*Notre Dame Integrated Imaging Facility, University of Notre Dame, Notre Dame, IN 46556, U.S.A.*
[3]*Department of Materials Science and Engineering, Cornell University, Ithaca, NY 14853, U.S.A.*

*E-mail: djena@cornell.edu

Received December 7, 2015; accepted February 23, 2016; published online April 25, 2016

We report tunable deep-ultraviolet (DUV) emission over the 222–231 nm range from 1–2 monolayer (ML) GaN quantum disks (QDs) grown in an AlN matrix. The linewidth of the emission were as narrow as ~10 nm at 5 K. The disks were grown in modified Stranski–Krastanov (mSK) mode. High resolution scanning transmission electron microscopy (STEM) images confirmed insertion of 1–2 MLs of GaN between 3 nm AlN barriers. The internal quantum efficiency was estimated from low temperature photoluminescence measurements for the disks, and compared with 1 and 2 ML GaN quantum wells/AlN barriers. The internal quantum efficiency (IQE) of the GaN QDs was found to be ~35% for 222 nm emission, ~200% higher than 1 ML GaN QWs. © 2016 The Japan Society of Applied Physics

1. Introduction

There is a strong demand for efficient deep-ultraviolet (DUV) LEDs and lasers for applications covering diagnostics, sensing and health care. The AlInGaN material family of alloys has the desired optical bandgaps to produce <280 nm DUV photons. Ternary AlGaN alloy quantum wells (QWs) have been used by several research groups[1–7] for this purpose, demonstrating emission wavelengths spanning 210–280 nm. Till date, however, the major challenge for this approach is the extremely low overall efficiency of such devices at short wavelengths.[8] The efficiency in LEDs is limited by carrier injection into the active region due to poor doping,[9,10] non-radiative recombination through defects, and inefficient light extraction originating from the optical polarization.[11] To improve the radiative efficiency by lowering the quantum confined stark effect (QCSE), use of ultra-thin GaN quantum structures has been proposed.[12–14] Use of a *binary* (GaN) material as the light emitting region has several potential advantages over ternary AlGaN alloys, provided the large blue shift required for DUV emission can be afforded by extreme quantum confinement. This is made feasible by the very large band offsets between AlN and GaN. A higher control of crystal growth and compositional homogeneity is expected. In this letter, we demonstrate tunable DUV emission from ultra-thin GaN quantum disks (QDs) below 230 nm grown using a modified Stranski–Krastanov (mSK) mode.[15–17] Also we show that the QDs are ~200% more efficient over QWs emitting at 222 nm.

We have grown ultra-thin GaN QDs in an AlN matrix to produce DUV emission over 222–231 nm range employing extreme quantum confinement. The 1–2 monolayer (ML) thick quantum disks were grown in a mSK mode. The epitaxial growths were performed using molecular beam epitaxy. The emission wavelength was tuned by changing the annealing time of the GaN layer. Transmission electron microscopy (TEM) analysis was performed to measure the thickness and composition of the quantum structures. The internal quantum efficiency (IQE) was measured using low temperature photoluminescence (LT PL) measurements. The IQE measured over the 222–231 nm range for the disks is ~35%, which is >2× higher compared to 1 ML GaN QWs emitting around 222 nm.

2. Experimental methods

A N_2-plasma assisted Veeco Gen-930 MBE system was used to grow the GaN disks and wells on AlN templates on Sapphire substrates with a typical threading dislocation density (TDD) of $1 \times 10^{10}\,cm^{-2}$. A 2-in. wafer was diced into $1 \times 1\,cm^2$ pieces, solvent cleaned, mounted on a Si wafer using indium, and loaded into the MBE chamber. Two outgassing bakes were performed at 200 °C for 7 h followed by 450 °C for 1.5 h. The samples were then transferred into the growth chamber consisting standard Al and Ga effusion cells. A N_2 plasma power of 400 W was used corresponding to a growth rate of ~260 nm/h. The chamber pressure was maintained at $\sim 2.1 \times 10^{-5}$ Torr, and a 10 rpm rotation was used. Surface conditions and growth modes were monitored in-situ using reflection high energy electron diffraction (RHEED).

The growth flow diagram is shown schematically in Fig. 1. An AlN nucleation layer is first grown on the substrate at 730 °C, at which the Al adatom mobility is low. At temperatures higher than 800 °C, significant decomposition of GaN occurs, making the GaN/AlN heterostructure growth difficult. Therefore we chose 730 °C as the growth temperature for both GaN and AlN. To counter the low Al adatom mobility, we used migration enhanced epitaxy (MEE). MEE involves alternate opening of Al and N_2 shutters for 30 s each to repeat three cycles of AlN formation. This corresponds to a ~6.5 nm AlN nucleation layer. After this layer, both Al and N_2 shutters were kept open to form ~24 nm AlN smooth film. This growth was kept in a slight metal-rich regime for a smooth surface, as confirmed by RHEED measurements. This step for the growth of smooth AlN is shown in Fig. 1(a). Before the deposition of GaN for the formation of quantum disks or wells, all the excess Al was consumed by opening only the N_2 shutter. The RHEED streaks were used as markers again to identify the Al consumption. To form GaN QDs on top of smooth AlN layers, a smooth two-dimensional (2D) GaN layer was first deposited as shown schematically in Fig. 1(b). The GaN growth condition was slightly metal-rich. This is in contrary to the commonly used SK growth condition, where 3D GaN islands are formed due to N_2-rich growth of GaN on AlN. After deposition of the smooth 2D GaN film, the layer is annealed at the growth temperature

© 2016 The Japan Society of Applied Physics

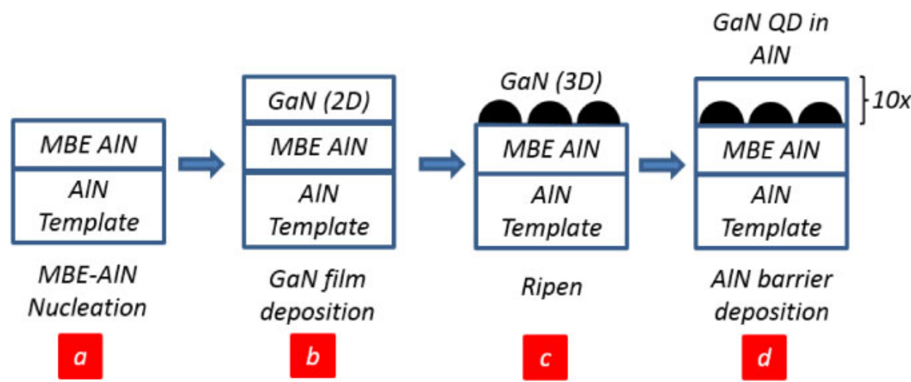

Fig. 1. (Color online) Schematic flow diagram for mSK growth method.

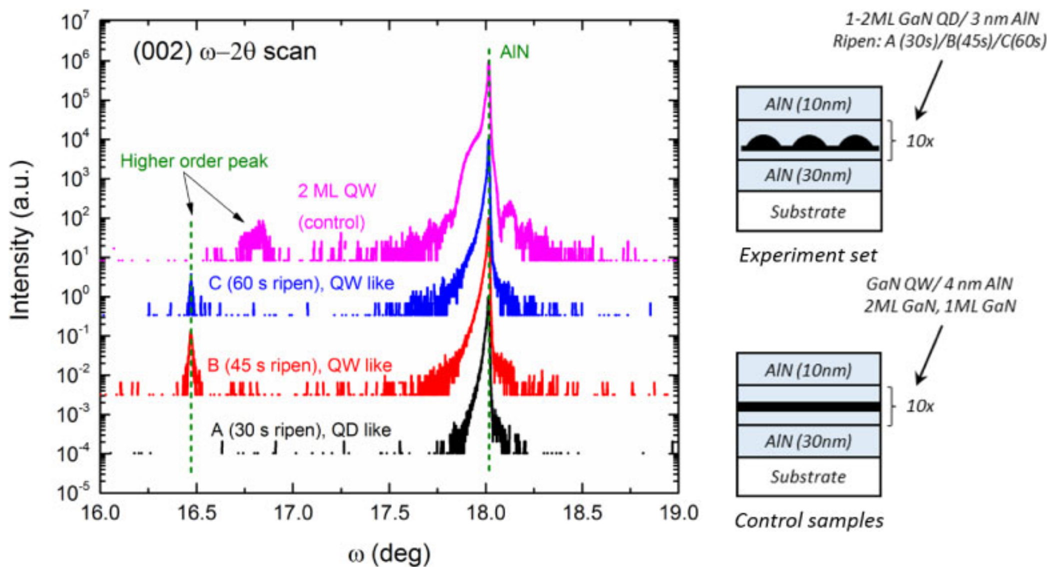

Fig. 2. (Color online) (002) ω–2θ triple axis HR-XRD analysis for QD samples (A/B/C) and the 2 ML QW control sample.

of 730 °C for a controlled amount of time, say t s. During this annealing process, the GaN layer partially decomposes, forming 3D islands, with a unique RHEED signature. We call this process "ripening" in this article [Fig. 1(c)]. This mechanism of formation of GaN QDs is a mSK mode. The GaN 3D islands are then capped with smooth AlN layers [Fig. 1(d)]. To counter the roughness of GaN QDs, the AlN layers are smoothened back using the MEE technique. Based on this mSK growth scheme, a series of three samples (A/B/C) were grown. 2 ML GaN layers were deposited in 3 nm AlN barriers for each sample, and this GaN/AlN heterostructure was repeated for 10 periods. The ripening time t was varied for the three samples: A (30 s) → B (45 s) → C (60 s). As control samples, two GaN QW/4 nm AlN barrier control samples were grown with GaN QW thickness of 1 and 2 ML *without* significant ripening ($t = 10$ s).

3. Results and discussion

Figure 2 shows the high-resolution X-ray diffraction (HR-XRD) triple axis (002) ω–2θ scans for the QD samples (A/B/C) and the 2 ML QW control sample. All samples show a strong AlN substrate peak. The QW sample shows satellite secondary peaks originating from coherent reflection from the smooth GaN layers. QD sample A does not show any such satellite peaks. QD samples B and C show satellite peaks like the QW samples suggesting that the GaN layers are more like QWs instead of QDs. This observation is explained by the thermal decomposition of the ultra-thin GaN layer at the growth temperature. The heterostructures were grown at a substrate temperature of 730 °C which is below the typical GaN decomposition temperature. But prolonged thermal anneal at this temperature can cause decomposition of fractional monolayers of GaN. The 30 s ripen (anneal) causes the top GaN monolayer to decompose and form fractional monolayer GaN disks. The bottom 1 ML is less affected and stays as a continuous wetting layer. The disks are randomly distributed which cause incoherent XRD and therefore the satellite XRD peak is absent for sample A. As the decomposition time is increased to 45 s for sample B, the decomposition of the GaN layer is enhanced leaving the 1 ML wetting layer exposed. Further ripening causes more exposure of this wetting layer. Therefore samples B and C have less scattering of the X-rays from the disks and can produce coherent diffraction that show up as the satellite peaks.

To investigate further the structural details, high-angle annular dark-field scanning transmission electron microscopy (HAADF-STEM) images were acquired for the QD samples A, B, and C as shown in Fig. 3. Sharp heterointerfaces are observed for all samples. The AlN barrier thicknesses are

© 2016 The Japan Society of Applied Physics

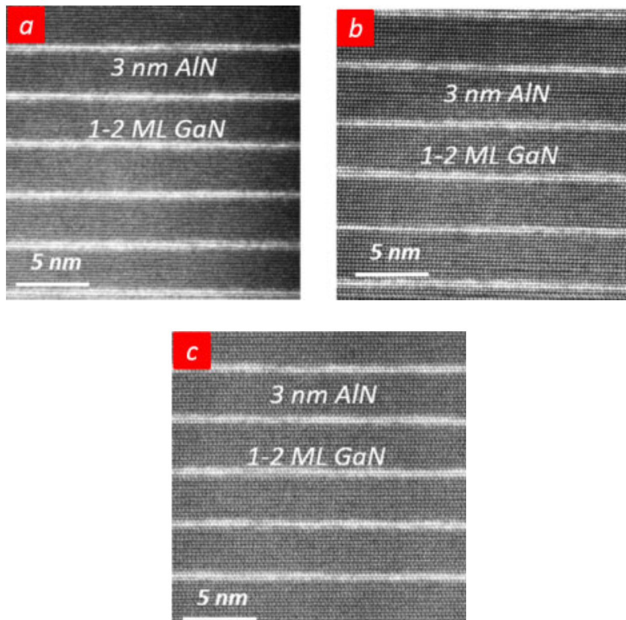

Fig. 3. (Color online) HAADF-STEM images for QD samples (a) A, (b) B, and (c) C.

3 nm. GaN QDs are 1–2 ML for all samples. No clear distinction is observed in this image for the GaN layers grown with different ripening times.

The optical properties were studied through PL using a 157 nm pulsed excimer laser excitation source. Temperature-dependent PL data was taken down to 5 K, shown in Fig. 4. Figure 4(a) is the spectra from the QW samples, and Fig. 4(b) for the QD samples. For the QW samples, strong single peaked emission were observed suggesting uniform 2D GaN layer distribution. The peak wavelength for 2 ML (1 ML) QW was 256 nm (222 nm) at 5 K. This value is consistent with the previously reported experimental data.[13] For QD samples, three distinct single peaked emissions were observed for samples A/B/C.

As the disk ripening time is increased from 30 s → 45 s → 60 s, the emission wavelength shows a monotonous blue shift from 231 nm → 227 nm → 222 nm at 5 K. This blue shift is described by the quantum confinement effect. As the ripening time is increased, the size of the QDs become smaller due to increased desorption of GaN, increasing the *lateral* quantum confinement. The measured full width at half maximum (FWHM) values are summarized in Table I. For the 1 ML (2 ML) QW samples, the widths were 9 nm (16 nm) at 5 K. The relatively wider emission for 2 ML QW might suggest some non-uniformity in the GaN layer thicknesses between the different periods. For the QD samples, the FWHM increases slightly from 11 nm → 12 nm → 13 nm between A → B → C. These widths suggest relatively uniform distribution of the QD sizes and slight increase in the randomness for the smaller QDs.

To estimate the IQE, temperature-dependent integrated PL measurements were performed. Figure 5 shows the trend of the temperature dependent IQE for the QD samples. The IQE values were calculated assuming saturation of all non-radiative recombination at 5 K. From the integrated PL intensity ratio ($I_{PL(300K)}/I_{PL(5K)}$), the highest IQE was measured for sample A (37%) and the lowest was for sample B (24%). Sample C showed an IQE of 36%. From

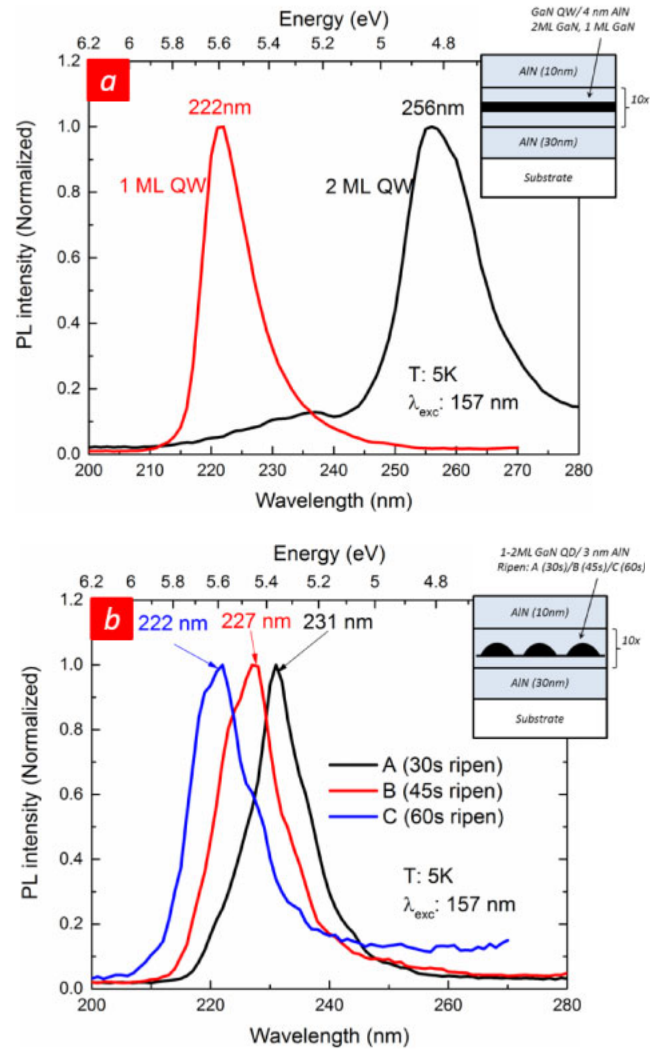

Fig. 4. (Color online) PL spectra measured at 5 K for (a) QW samples (b) QD samples.

Table I. Comparison of optical properties between QW and QD samples.

Sample	GaN thickness (ML)	λ_p (nm)	FWHM (nm)	IQE (%)
A	1–2	231	11	37
B	1–2	227	12	24
C	1–2	222	13	36
QW-1	1	222	9	17
QW-2	2	256	16	49

the IQE(T) distribution of Fig. 5, the IQE drop starts at the lowest temperature for sample A. The activation energy for non-radiative processes is the highest for sample C (222 nm) and is the lowest for sample A (231 nm), meaning the smaller QDs are thermally more robust. The quantum confinement serves two purposes: it shortens the emission wavelength by increasing the effective bandgap, and it also isolates the QDs from the non-radiative recombination centers through an energy barrier, increasing the IQE.

Finally, we compare the IQE between QDs and the QW control samples. The IQE trend vs emission wavelength is shown in Fig. 6. For QWs, the IQE decreases from 49% (2 ML) to 17% (1 ML) at shorter wavelengths. This decrease can be due to carrier escape into barriers from shallower

© 2016 The Japan Society of Applied Physics

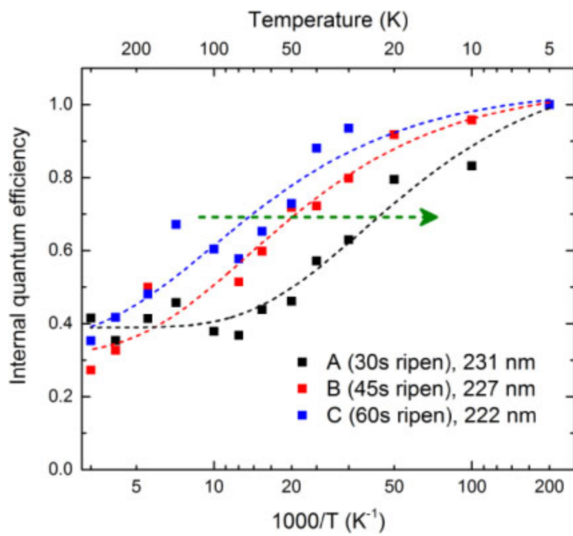

Fig. 5. (Color online) Temperature dependent integrated PL intensity for IQE estimation.

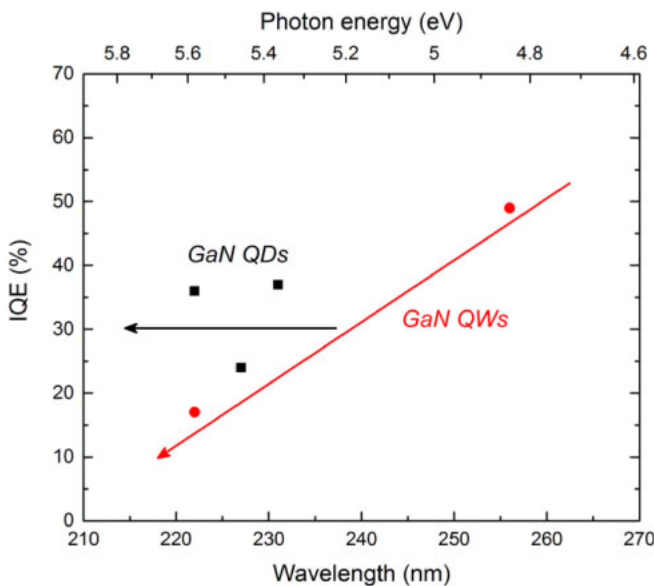

Fig. 6. (Color online) IQE comparison between QD and QW samples.

quantum wells for 222 nm emission compared to 256 nm. For the QD samples, we see that the IQE stays around 35% for the whole range of 222–231 nm emission, ~200% higher than 1 ML GaN QWs at 222 nm. This comparative efficiency boost also suggests enhanced 3D quantum confinement.

4. Conclusions

We have observed tunable DUV emission from 1–2 ML GaN QDs in AlN barriers grown in mSK mode below 230 nm. The emission wavelength could be tuned by controlling the annealing time of the GaN disks. The FWHM was narrow (11–13 nm) over the entire range of emission of 222–231 nm. IQE from temperature dependent PL measurements for GaN QDs show a ~200% increase over wells. Active regions incorporating such disks with extreme quantum confinement can potentially enable efficient DUV light emitters with high efficiencies.

Acknowledgement

The authors would like to thank NSF-DMREF to support this work.

1) S. Nakamura, in *Gallium Nitride (GaN) I*, ed. J. I. Pankove and T. D. Moustakas (Academic Press, New York, 1998) Semiconductors and Semimetals, Vol. 50, Chap. 14.
2) T. D. Moustakas, in *Gallium Nitride (GaN) II*, ed. J. I. Pankove and T. D. Moustakas (Academic Press, New York, 1999) Semiconductors and Semimetals, Vol. 57, Chap. 2.
3) Y. Taniyasu, M. Kasu, and T. Makimoto, Nature **441**, 325 (2006).
4) A. Khan, K. Balakrishnan, and T. Katona, Nat. Photonics **2**, 77 (2008).
5) C. Pernot, M. Kim, S. Fukahori, T. Inazu, T. Fujita, Y. Nagasawa, A. Hirano, M. Ippommatsu, M. Iwaya, S. Kamiyama, I. Akasaki, and H. Amano, Appl. Phys. Express **3**, 061004 (2010).
6) H. Hirayama, Y. Tsukada, T. Maeda, and N. Kamata, Appl. Phys. Express **3**, 031002 (2010).
7) M. Shatalov, W. Sun, A. Lunev, X. Hu, A. Dobrinsky, Yu. Bilenko, J. Yang, M. Shur, R. Gaska, C. Moe, G. Garrett, and M. Wraback, Appl. Phys. Express **5**, 082101 (2012).
8) M. Kneissl, T. Kolbe, C. Chua, V. Kueller, N. Lobo, J. Stellmach, A. Knauer, H. Rodriguez, S. Einfeldt, Z. Yang, N. M. Johnson, and M. Weyers, Semicond. Sci. Technol. **26**, 014036 (2011).
9) P. Kozodoy, M. Hansen, S. P. DenBaars, and U. K. Mishra, Appl. Phys. Lett. **74**, 3681 (1999).
10) J. Simon, V. Protasenko, C. Lian, H. Xing, and D. Jena, Science **327**, 60 (2010).
11) K. B. Nam, J. Li, M. L. Nakarmi, J. Y. Lin, and H. X. Jiang, Appl. Phys. Lett. **84**, 5264 (2004).
12) J. Verma, P. Kandaswamy, V. Protasenko, A. Verma, H. Xing, and D. Jena, Appl. Phys. Lett. **102**, 041103 (2013).
13) Y. Taniyasu and M. Kasu, Appl. Phys. Lett. **99**, 251112 (2011).
14) J. Verma, S. M. Islam, V. Protasenko, P. Kumar Kandaswamy, H. G. Xing, and D. Jena, Appl. Phys. Lett. **104**, 021105 (2014).
15) J. S. Brown, P. M. Petroff, F. Wu, and J. S. Speck, Jpn. J. Appl. Phys. **45**, L669 (2006).
16) J. Renard, P. K. Kandaswamy, E. Monroy, and B. Gayral, Appl. Phys. Lett. **95**, 131903 (2009).
17) F. Widmann, J. Simon, B. Daudin, G. Feuillet, J. L. Rouvière, N. T. Pelekanos, and G. Fishman, Phys. Rev. B **58**, R15989(R) (1998).

© 2016 The Japan Society of Applied Physics